Nanoscale

PAPER

View Article Online
View Journal

Cite this: DOI: 10.1039/d5nr05395a

Closing the nitrogen loop: sustainable ammonia production from industrial nitrate waste using a stacked electrolyzer

Paulraj Gnanasekar, †[a] Gowthambabu Vellingiri,†[a,b] Murtadha J. AlTammar,[c] Karthik Peramaiah,[d] Jeganathan Kulandaivel,[b] Boon S. Ooi,[a] Abeer A. Alarawi*[c] and Tien Khee Ng *[a]

Received 22nd December 2025,
Accepted 30th April 2026

DOI: 10.1039/d5nr05395a

rsc.li/nanoscale

Nitrate in wastewater poses a significant threat to the aquatic ecosystem and disrupts the nitrogen cycle. In this study, we developed a stacked electrolyzer capable of converting nitrate in industrial effluents, even at low concentrations, into green ammonia (NH_3) through the nitrate reduction reaction. Our catalyst synergistically transforms the nitrates into vital intermediates (NO_x), which are then further reduced to NH_3. The stacked electrolyzer achieved a faradaic efficiency of 37% and an NH_3 yield of ~7.8 mg h^{-1} when treating low-concentration industrial wastewater (1000 ppm). Additionally, it demonstrated a wastewater processing capacity of 5 L day^{-1} with a single-pass ammonia recovery of 27.7%. Overall, our approach of producing green ammonia from nitrate-laden effluents represents a promising solution for closing the nitrogen cycle.

Introduction

With its potential as a sustainable fuel and its huge requirement in the agricultural and industrial sectors, the demand for ammonia (NH_3) continues to grow, boasting a compound annual growth rate (CAGR) of 5–7%.[1,2] Currently, the global demand is met primarily through the Haber–Bosch (HB) process, which combines hydrogen (produced *via* methane steam reforming) and nitrogen at high temperatures and pressures, resulting in approximately 450 million metric tons of CO_2 emissions annually.[3] Recent developments in green ammonia production have demonstrated that the nitrate reduction reaction (NO3RR) method can achieve nearly 100% faradaic efficiency and excellent stability. This efficiency significantly surpasses those of nitrogen reduction reactions and lithium-mediated and plasma-assisted nitrogen reduction, primarily due to its lower energy barrier to break N–O.[4–6] In general, the NO3RR is typically conducted at the laboratory scale using nitrate salts such as $NaNO_3$ and KNO_3, which are predominantly synthesized through the oxidation of ammonia in the industrial Ostwald process.[7] NH_3 production *via* the NO3RR using synthetic nitrate sources is valuable for assessing a catalyst's activity, selectivity, and stability. However, this method alone is not practical for large-scale NH_3 synthesis. The NO3RR pathway becomes more compelling when nitrates are sourced from atmospheric NO_x capture or from nitrate-rich wastewater streams. On the other hand, nitrate pollutants are some of the life-threatening pollutants released into water resources, and they are commonly observed in industrial and household wastewater, as well as in agricultural runoff (23 million metric tons).[8–15]

Various methods are employed to degrade nitrate pollutants in industrial wastewater, such as the activated sludge process,[16] membrane aerated biofilm reactors,[17] electrodialysis,[18] nitrate reduction,[19] and reverse osmosis.[20] These approaches convert nitrate into nitrogen and release it into the atmosphere at a high purification cost.[21,22] Towards achieving sustainability, one of the most promising solutions is converting nitrate in industrial wastewater into green ammonia with the help of renewable energy. This approach helps produce green ammonia by recovering harmful nitrate pollutants and thus significantly reducing the CO_2 emissions associated with traditional degradation processes.

The concentration of nitrate pollutants in real-world scenarios is typically low, around 2000 ppm (2 g L^{-1}). Most reported catalysts have been tested at higher nitrate concentrations, such as 0.1 or 0.5 M, under laboratory conditions.[23,24] On the other hand, some of the studies have

[a]*Photonics Laboratory, Computer, Electrical and Mathematical Sciences and Engineering, CEMSE Division, King Abdullah University of Science and Technology (KAUST), Thuwal - 23955, Saudi Arabia. E-mail: tienkhee.ng@kaust.edu.sa*
[b]*Center for Nanoscience and Nanotechnology, Department of Physics, Bharathidasan University, Tiruchirappalli-620024, Tamil Nadu, India*
[c]*Upstream Advanced Research Center, Saudi Aramco, Dhahran - 31311, Saudi Arabia*
[d]*Institute of Sustainability for Chemicals, Energy and Environment (ISCE²), Agency for Science, Technology and Research (A*STAR), Singapore – 627833, Singapore*
†These authors equally contributed.

also demonstrated the NO3RR at lower concentrations and encountered a strong counter hydrogen evolution reaction (HER), due to the limited availability of nitrate.[25–30] For efficient conversion of real-world nitrate pollutants, particularly at low concentrations, the stacked electrolyzer approach is highly advantageous. This configuration enables high-volume wastewater processing and enhanced nitrate degradation, making it well-suited for scalable ammonia production. Furthermore, identifying efficient and stable catalysts for the NO3RR in stacked electrolyzers under low-concentration nitrate wastewater conditions remains a significant challenge for scaling up the process toward practical, large-scale applications.

Recently, CuO and AgO-based catalysts have demonstrated promising activity for nitrate reduction, particularly under relatively low concentration conditions.[31–34] In this context, CuO-based materials are widely recognized for their ability to facilitate the conversion of nitrate into ammonia, even at reduced nitrate levels.[35] Conversely, AgO-based catalysts exhibit a strong tendency to promote the formation of key intermediates such as nitrite (NO_2^-), which plays a crucial role in the multi-step reaction pathway towards ammonia.[33] While these studies highlight the individual catalytic metrics of CuO and AgO systems, most investigations have primarily focused on material-level optimization under batch conditions and at relatively high nitrate concentrations, limiting their direct applicability to practical wastewater treatment scenarios.

In contrast, the present work advances beyond conventional approaches by introducing a system-level strategy that integrates CuO/AgO nanoparticles within a stacked electrolyzer configuration operating under continuous-flow conditions. This study specifically targets the treatment of low-concentration industrial wastewater (1000 ppm) using a single-pass flow system, thereby addressing a critical gap between laboratory-scale studies and real-world applications. Furthermore, the designed system enables the simultaneous reduction of nitrate and recovery of ammonia, shifting the focus from pollutant removal to nitrogen resource recovery.

In this research work, we have demonstrated a stacked electrolyzer using the CuO/AgO catalyst for the recovery of low-concentration nitrate as NH_3 from industrial wastewater (1000 ppm). In our two-stack electrolyzer with an active area of 50 cm^2, we have observed a faradaic efficiency (FE) of 42.5% for lab nitrate pollutants ($NaNO_3$) and an FE of 37% for industrial wastewater. Most importantly, the energy conversion efficiency was calculated to be 13.5% for the industrial wastewater NO3RR. Additionally, our stacked electrolyzer demonstrated industrial wastewater nitrate degradation at 5 L day^{-1}, with a single-pass nitrate recovery efficiency of 27.6%.

Results and discussion

Morphological and chemical characterization

A schematic illustration of the catalyst preparation is given in Fig. 1a & Scheme S1 and discussed in detail in the SI. FESEM images of CuO and AgO NPs show rice-like cylindrical structures and spherical nanoparticles with average particle sizes ranging from 140–150 nm and 200–220 nm, respectively (Fig. 1b, S4 and S5). Furthermore, EDS elemental mapping confirms the formation of CuO and AgO nanoparticles and evidences the uniform presence of CuO and AgO NPs on the GDL (Fig. 1c–g, S6 and S7). In addition, in the XRD spectra (Fig. S8) of CuO, 2θ peaks are observed at 32.5° (110), 35.48° (002), 37.74° (111), 48.75° (202), 53.46° (020), 58.17° (202), 61.46° (113), 66.00° (311), and 67.82° (220) and for AgO 2θ peaks are observed at 38.08° (111), 64.4° (220), and 65.5° (222), all of which are in good agreement with the reported literature[34,35] and JCPDS card number 45-0937 (CuO NPs) and 76-1393 (AgO NPs). Additionally, two peaks were observed for Ag_2O (JCPDS card number 76-1393) at 32.89° (111) and 55.11° (220).[35]

Furthermore, the XPS survey spectrum of CuO/AgO (Fig. S9) confirms the presence of Cu, Ag, O and C elements. The high-resolution Cu 2p spectrum (Fig. 1h) was deconvoluted into Cu $2p_{3/2}$ peaks at 933.75 eV (Cu^+) and 935.17 eV (Cu^{2+}) along with Cu $2p_{1/2}$ peaks at 953.6 eV (Cu^+) and 955.16 eV (Cu^{2+}), confirming the coexistence of mixed oxidation states.[36] The Ag core-level spectrum (Fig. 1i) shows characteristic Ag $3d_{5/2}$ and Ag $3d_{3/2}$ peaks at 367.8 eV and 374.54 eV, respectively, corresponding to Ag^+/Ag^0 species. The O 1s spectrum (Fig. 1j) exhibits a dominant metal–oxygen (M–O) peak centered at 530.2 eV, which can be attributed to both Cu–O and Ag–O bonds.[37] Additionally, the C 1s spectrum (Fig. 1k) displays multiple components corresponding to C–C (284.7 eV), C–O–C (285.8 eV), π–π* (291.7 eV), and CF_3 (292.8 eV) functionalities. The C–C and π–π* peaks arise predominantly from the carbon paper substrate, while the oxygenated carbon species and CF_3 peaks are associated with the Nafion binder, confirming its presence on the electrode surface.

Importantly, the coexistence of Cu^+/Cu^{2+} and Ag^0/Ag^+ oxidation states suggests a synergistic electronic interaction within the CuO/AgO heterostructure. Cu mixed-valence configurations are known to enhance electrocatalytic activity by facilitating charge transfer and optimising adsorption energies of reaction intermediates.[38] Specifically, Cu^{2+} species provide active sites for adsorption of oxygenated intermediates (*e.g.*, *OH, *O), while Cu^+ species contribute to improved electrical conductivity and charge delocalisation.[37] Concurrently, metallic Ag^0 enhances electron mobility, whereas Ag^+ species participate in surface redox transitions under operating conditions.[39]

Furthermore, the presence of these redox-active species indicates the possibility of dynamic surface reconstruction during electrochemical operation, where reversible interconversion between Cu^+/Cu^{2+} and Ag^0/Ag^+ states can occur. Such a phenomenon has been widely reported to improve catalytic durability by maintaining active surface sites under prolonged reaction conditions.[40] From an electronic structure perspective, the mixed-valence environment can modulate the d-band centre, thereby optimising the adsorption strength of key intermediates and lowering reaction energy barriers, leading to enhanced catalytic kinetics.[41] Overall, this analysis not only confirms the successful formation of CuO/AgO on the carbon

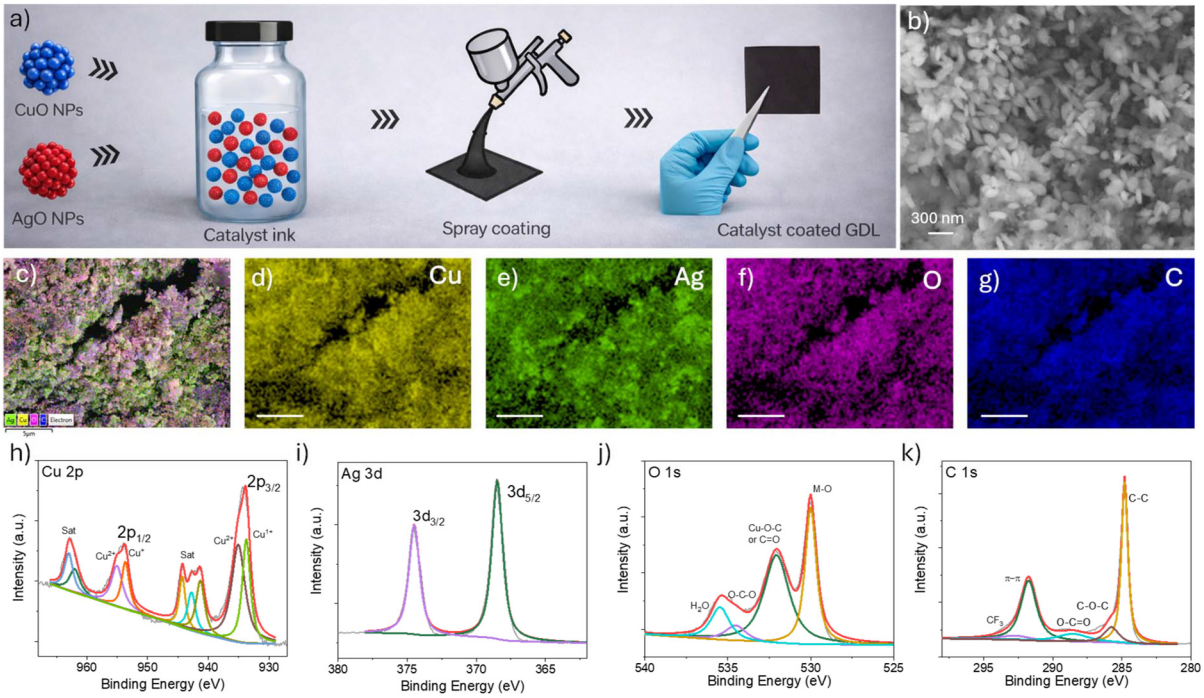

Fig. 1 (a) Schematic illustration of the preparation of a CuO/AgO catalyst-coated gas diffusion layer (GDL) through catalyst ink preparation and the spray coating method, (b) FESEM images of the CuO/AgO NP coated GDL, (c–g) EDS elemental mapping of the CuO/AgO coated GDL, and (h–k) XPS core-level binding energy spectrum of Cu, Ag, O, and C, respectively.

paper substrate but also reveals a mixed-valence, electronically coupled system that is highly favourable for improved electrocatalytic activity and stability. The morphological and chemical characterization studies collectively confirm the uniform distribution of CuO/AgO on the GDL, providing abundant active sites and efficient charge transport pathways.

Electrochemical nitrate reduction reaction

We evaluated the electrochemical NO3RR performance of the CuO/AgO catalyst at various nitrate concentrations through current–voltage measurements, as shown in Fig. 2a. The results clearly indicate that the current density increases with higher nitrate concentrations, demonstrating the selectivity of the CuO/AgO catalyst towards the nitrate reduction reaction.[42,43] Additionally, chronopotentiometry (CP) analysis at various nitrate concentrations (Fig. S10) confirmed the NH_3 selectivity of the CuO/AgO catalyst, with the maximum NH_3 production reaching 196 μg h^{-1} cm^{-2} and an FE_{NH3} of 4.6% at a concentration of 25 mM $NaNO_3$ (Fig. 2b). Furthermore, we observed an increase in NO_2 formation as NO_3 concentration increased under the test conditions (Fig. S11). This is likely related to the formation of intermediates, which can subsequently be reduced to NH_3 over time.[31]

In this typical electrochemical process, AgO acts as the primary active site for nitrate adsorption and its initial two-electron reduction to nitrite (NO_2^-), owing to its strong affinity for nitrate species. This step is critical, as nitrite serves as a key intermediate in the pathway toward NH_3 formation. Subsequently, CuO facilitates the further reduction of nitrate to NH_3 through successive proton-coupled electron transfer steps. Cu-based sites provide favourable adsorption energies for nitrogen-containing intermediates, thereby enhancing NH_3 selectivity while suppressing competing reactions such as the HER. Importantly, the intimate interfacial contact between CuO and AgO enables rapid transfer of intermediates (NO_2^-) between active sites, minimising intermediate accumulation and improving overall reaction kinetics. This is particularly beneficial at ultra-low nitrate concentrations, where efficient utilisation of intermediates is critical to maintain high conversion efficiency. Overall, the CuO/AgO system exhibits a clear synergistic effect, where CuO initiates nitrate activation and AgO drives the subsequent reduction to NH_3. This cooperative mechanism enhances FE, improves selectivity and enables an effective NO_3 to NH_3 conversion rate even at low concentrations.

To mimic the typical effluent conditions, we conducted the NO3RR at 2000 ppm NO_3 in 0.1 M KOH (Fig. S12).[44,45] To identify the optimal current density for long-term operation, we performed CP at various applied currents (Fig. 2c and S13). At higher current densities, we achieved a notable NH_3 production rate of 1.1 mg h^{-1} cm^{-2} at 200 mA cm^{-2}, along with a maximum FE_{NH3} of 15% at 50 mA cm^{-2}. The corresponding NO_2^- yield and FE are shown in Fig. S14. These results indicate its potential for real-world nitrate contaminant conversion to ammonia. Crucially, the NMR results of the $^{15}NO_3$ isotope control experiments also confirm that the ammonia formation

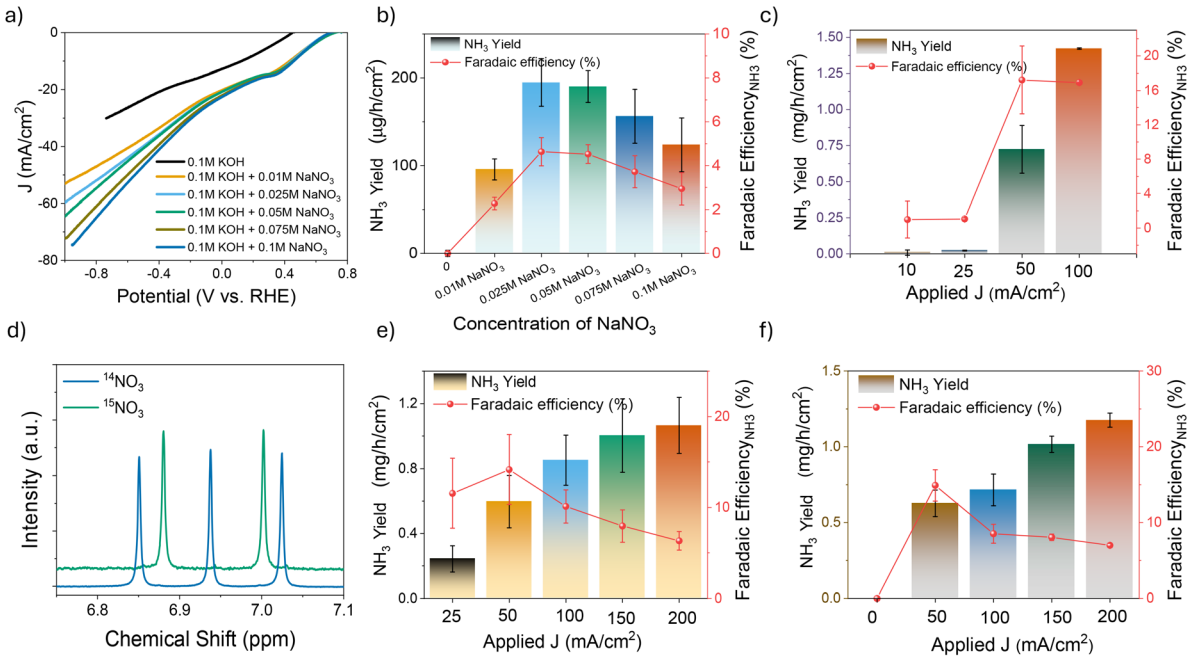

Fig. 2 (a) Linear sweep voltammetry analysis of CuO/AgO at various nitrate concentrations, (b) NH_3 yield and the corresponding faradaic efficiency of the CuO/AgO catalyst with an applied current density of 50 mA cm^{-2} at various nitrate concentrations, (c) NO3RR performance of CuO/AgO at 2000 ppm $NaNO_3$, (d) $^{15}NO_3$ isotope labelling control experiment, and (e and f) electrolyzer assisted NO3RR performance of CuO/AgO at 2000 ppm NO_3 concentration under 0.1 M KOH and DI water conditions.

is from the nitrate source rather than the contamination from the electrolyte or catalyst (Fig. 2d).[46,47]

The electrolyzer-assisted green fuel production has been demonstrated as the most promising approach for large-scale applications. Here, we examined the NO3RR performance using a membrane electrode assembly (MEA) (fabrication of MEA is discussed in the SI) with a low nitrate concentration of 2000 ppm, in both 0.1 M KOH and deionized (DI) water. We evaluated the performance across various current densities and flow rates (see Fig. S15–22). Under 0.1M KOH electrolyte conditions, a current density of 50 mA cm^{-2} and a flow rate of 15 mL min^{-1} were identified as the optimum parameters (Fig. 2e). Similarly, in DI water, the highest FE_{NH3} was recorded at 50 mA cm^{-2} with a flow rate of 15 mL min^{-1} (Fig. 2f). Importantly, we noted a significantly high concentration of NO_2^-, which may be associated with the NO_3 reduction to NO_2^- performance of the AgO nanoparticles (Fig. S17 and S22).[32]

Towards the real-time application, we tested the NO3RR at a very low NO_3 concentration of 1000 ppm using a single-pass approach at a current density of 50 mA cm^{-2} and a flow rate of 15 mL min^{-1} for a duration of 100 hours (see Fig. 3b and S23). As illustrated in Fig. 3b, we observed an FE_{NH3} of 45%, with an energy conversion efficiency (ECE)[48] of 25.31% and an NH_3 production rate of 1.9 mg h^{-1} cm^{-2}. Additionally, we assessed the nitrate conversion efficiency, which was found to be 33.13% in the single-pass approach. This can be further improved by a stacked electrolyzer approach.[49] Towards the goal of a sustainable future, degradation of nitrate in industrial effluents was demonstrated using a stacked electrolyzer[50,51] with an active area of 50 cm^2 (details about the development of our stacked electrolyzer are provided in the SI) and schematically illustrated in Fig. 3a. The industrial wastewater we received from Aramco, Saudi Arabia, had very negligible nitrate contamination. To simulate contaminated water, we included 1000 ppm of nitrate in our testing. To provide better context, the composition of the collected industrial wastewater was analysed using ion chromatography (IC) and the results are shown in Fig. S25. The analysis indicates that chloride ions are the dominant species, while nitrate, phosphate and sulphate concentrations are initially negligible prior to external incorporation. The developed stacked electrolyzer was tested at a current density of 25 mA cm^{-2} with a flow rate of 5 ml min^{-1}, as shown in Fig. 3d. The ammonia yield was estimated to be 300 mg after 50 hours, with an FE_{NH3} of 37% and an ECE_{NH3} of 13.41% (Fig. 3c and S26). The decrease in ECE and FE observed under industrial wastewater conditions, compared to lab conditions, is attributed to counter-reactions occurring in real-world wastewater. Notably, the degradation rate was nearly 5 L day^{-1} for the tested two-stack electrolyzer with a nitrate conversion percentage of 27.63%. It is important to highlight that both conversion efficiency and ammonia yield can be further improved by using stacked electrolyzers and optimising the operational parameters. Post-morphological analysis and inductively coupled plasma (ICP) results confirm the absence of catalyst leaching (Fig. S27 & Table S1) and evidence the catalyst durability.

The reduction of nitrate to NH_3 at an ultra-low concentration has been achieved through the synergistic effects of

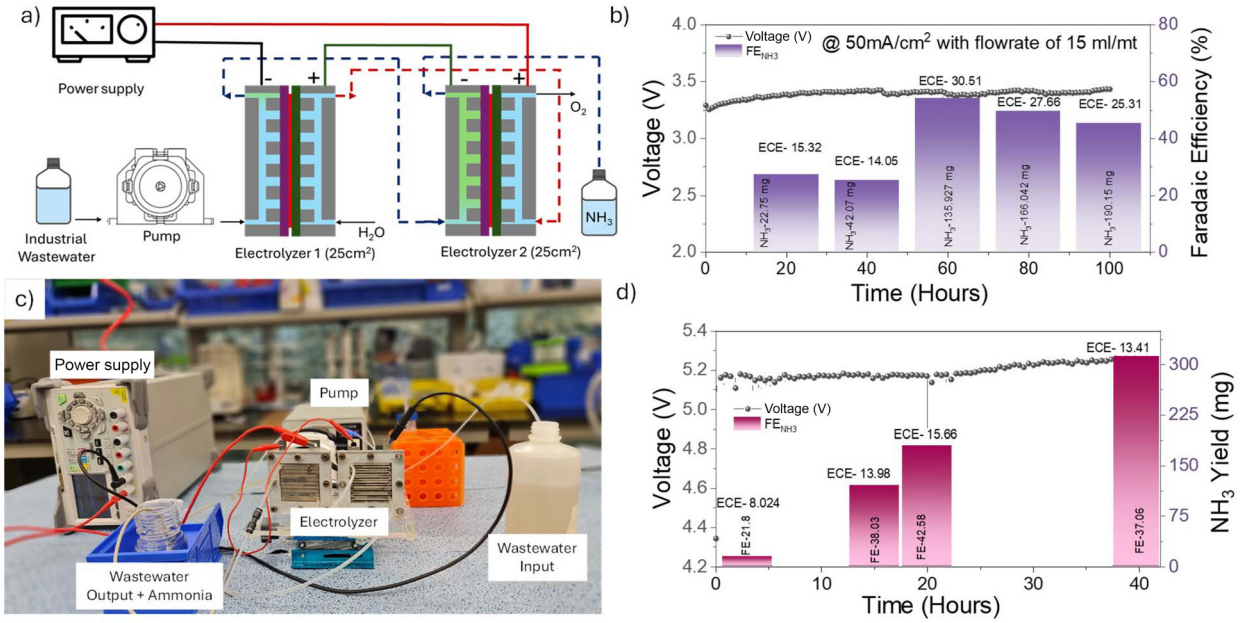

Fig. 3 (a) Schematic illustration of the stacked electrolyzer analysis, (b) NH_3 yield and FE_{NH3} for long-term low concentration NO3RR with 1000 ppm concentration at 50 mA cm^{-2}, (c) digital image of the wastewater NO3RR in a stacked electrolyzer, and (d) NH_3 yield and FE_{NH3} for long-term low concentration NO3RR with 1000 ppm concentration at 25 mA cm^{-2}.

CuO and AgO catalysts. In this process, the AgO catalyst is essential for converting NO_3^- into NO_2^-, an important intermediate. Subsequently, the CuO NPs facilitate the conversion of nitrite into NH_3. This study explores the potential of transforming nitrate-rich industrial wastewater into a sustainable resource for NH_3 production.

To further contextualize the performance of the present system, a comparative analysis with recently reported NO3RR catalysts is summarized in Table S2. As shown, most literature reports employ batch-type H-cells or conventional flow cells at relatively high nitrate concentrations, achieving high faradaic efficiencies (typically > 60%). In contrast, the present CuO/AgO system operates under practically relevant conditions, utilising real industrial wastewater (1000 ppm) in a stacked electrolyzer configuration with continuous single-pass operation.

Despite the inherently challenging low-concentration regime, the proposed system achieves a faradaic efficiency of ~37% and low energy conversion efficiency, which is comparable when considering the significant differences in operating conditions. More importantly, this proof-of-concept demonstrates several key advancements over existing studies: (i) the implementation of a stacked-electrolyzer architecture, enabling improved scalability and continuous processing; (ii) effective nitrate reduction under dilute conditions, which remains largely underexplored; and (iii) the simultaneous recovery of ammonia, contributing towards nitrogen resource utilization rather than simple pollutant removal.

These distinctions highlight that, unlike conventional studies focused primarily on maximizing catalytic efficiency under idealized conditions, the present work emphasizes a system-level, application-oriented approach, thereby bridging the gap between laboratory-scale catalyst development and realistic wastewater treatment scenarios.

Based on our techno-economic analysis (see the SI), the estimated cost of recovering NH_3 from wastewater containing 1000 ppm NO_3^- is higher than the cost of conventionally produced ammonia *via* the HB process, and the recovery route offers a more sustainable alternative from an environmental perspective. Instead of allowing NO_3^- to simply convert into N_2 as a byproduct, this approach enables the selective conversion of nitrates into valuable NH_3, promoting efficient nitrogen recovery and supporting a circular nitrogen economy. While promising, there remains substantial room for improvement through catalyst optimization, integration of nitrate concentration technologies (such as electrodialysis), and the development of stacked electrolyzer systems to enhance overall efficiency and scalability. On the other hand, when compared to electrochemical direct nitrogen reduction to NH_3, the nitrate to NH_3 recovery process offers a lower production cost,[52] highlighting its practicality and benefits for both water treatment and NH_3 recovery. Conventional processes typically focus only on removing NO_3^- by converting it into nitrogen gas,[53–59] whereas our approach captures and converts nitrate into valuable NH_3. This not only enables the sustainable production of green NH_3 but also supports environmental protection by reducing carbon emissions and preventing nitrate pollution in aquatic ecosystems.

Overall, this integrated method presents a sustainable and circular solution that addresses both clean ammonia production and environmental remediation, aligning with global goals for decarbonization and water resource preservation. By bridging the gap between laboratory-scale catalyst design and

system-level industrial application, this work establishes a viable pathway for transforming nitrate pollutants into a valuable nitrogen resource.

Conclusion

An efficient CuO/AgO NPs catalyst has been successfully synthesized, demonstrating strong performance in reducing nitrate at ultra-low concentrations. Additionally, a stacked electrolyzer system was developed to address nitrate contamination in real-world industrial wastewater, converting it into green ammonia. In a single pass, the system achieved a 27% single-pass conversion efficiency at a treatment rate of 5 L day^{-1}. Post-reaction ICP analysis and morphological characterization confirmed the catalyst's structural integrity, indicating no degradation and supporting its long-term stability. Importantly, this study advances beyond conventional batch systems by demonstrating NO_3^- to NH_3 conversion in a realistic, dilute wastewater matrix, thereby addressing a critical gap between laboratory studies and practical implementation. While further improvements in efficiency and selectivity are required, this work provides a successful proof-of-concept for nitrogen recovery from dilute wastewater. The CuO/AgO-based continuous-flow system enables NO_3^- to NH_3 conversion, representing a practical step toward closing the nitrogen loop and advancing sustainable, resource-efficient wastewater treatment technologies.

Author contributions

Paulraj Gnanasekar: conceptualization, catalyst synthesis, data interpretation, analysis, and original manuscript writing. Gowthambabu Vellingiri: catalyst synthesis, data interpretation, and analysis. Abeer A. Alarawi: conceptualization and manuscript revision. Murtadha J. AlTammar: conceptualization and manuscript revision. Karthik Peramaiah: data analysis, data interpretation, and manuscript revision. Tien Khee Ng: supervision, data interpretation, manuscript revision, procurement, and project management. Jeganathan Kulandaivel: data interpretation and manuscript revision. Boon S. Ooi: conceptualization, supervision, data analysis, project management and manuscript revision.

Conflicts of interest

There are no conflicts to declare.

Data availability

The data that support the findings of this study are available from the corresponding author upon reasonable request.

Supplementary information (SI) is available. See DOI: https://doi.org/10.1039/d5nr05395a.

Acknowledgements

PG, TK, and BO would like to thank King Abdullah University of Science and Technology (KAUST) for the baseline funding (BAS/1/1614-01-01). They also acknowledge Aramco for supporting the research through an external grant (RGC/3/5694-01-01). PG and GV acknowledge the KAUST Imaging and Characterization Core Labs and the Prototyping Core Labs for the characterization and prototyping facilities. GV gratefully acknowledges the KAUST for the Visiting Scholar Program. GV and JK thank the Ministry of Education – RUSA 2.0 (R&I) Physical Sciences for their support.

References

1 P. H. van Langevelde, I. Katsounaros and M. T. M. Koper, *Joule*, 2021, **5**, 290–294.
2 M. Wang, M. A. Khan, I. Mohsin, J. Wicks, A. H. Ip, K. Z. Sumon, C.-T. Dinh, E. H. Sargent, I. D. Gates and M. G. Kibria, *Energy Environ. Sci.*, 2021, **14**, 2535–2548.
3 S. Yin, R. Cao, Y. Han, J. Shang, J. Zhang, W. Jiang and G. Liu, *J. Energy Chem.*, 2024, **96**, 642–668.
4 T. Sakakura, S. Uemura, M. Hino, S. Kiyomatsu, Y. Takatsuji, R. Yamasaki, M. Morimoto and T. Haruyama, *Green Chem.*, 2018, **20**, 627–633.
5 W. Chang, A. Jain, F. Rezaie and K. Manthiram, *Nat. Catal.*, 2024, **7**, 231–241.
6 H. M. Nguyen, A. Omidkar, W. Li, S. Meng, Z. Li and H. Song, *Chem. Eng. J.*, 2023, **471**, 144748.
7 H. Huang, K. Peramaiah and K.-W. Huang, *Energy Environ. Sci.*, 2024, **17**, 2682–2685.
8 B. Singh and E. Craswell, *SN Appl. Sci.*, 2021, **3**, 518.
9 Y. A. Kumar and H.-J. Kim, *New J. Chem.*, 2018, **42**, 19971–19978.
10 S. A. Hira, S. Nagappan, D. Annas, Y. A. Kumar and K. H. Park, *Electrochem. Commun.*, 2021, **125**, 107012.
11 A. K. Yedluri and H.-J. Kim, *Dalton Trans.*, 2018, **47**, 15545–15554.
12 G. Vellingiri, M. Jothi, P. Gnanasekar, T. K. Ng, B. S. Ooi and J. Kulandaivel, *Langmuir*, 2025, **41**, 32534–32545.
13 A. Dixit, J. A. Abraham, M. Manzoor, M. Altaf, Y. A. Kumar and R. Sharma, *Mater. Sci. Eng., B*, 2024, **307**, 117530.
14 K. D. Kumar, Y. A. Kumar, T. Ramachandran, A. A. Al-Kahtani and M. Kang, *Mater. Sci. Eng., B*, 2023, **296**, 116715.
15 K. D. Kumar, T. Ramachandran, Y. A. Kumar, A. A. A. Mohammed and M. Kang, *J. Phys. Chem. Solids*, 2024, **185**, 111735.
16 V. Matějů, S. Čižinská, J. Krejčí and T. Janoch, *Enzyme Microb. Technol.*, 1992, **14**, 170–183.
17 E. Syron and E. Casey, *Environ. Sci. Technol.*, 2008, **42**, 1833–1844.
18 A. El Midaoui, F. Elhannouni, M. Taky, L. Chay, M. A. M. Sahli, L. Echihabi and M. Hafsi, *Sep. Purif. Technol.*, 2002, **29**, 235–244.

19 Z.-Y. Wu, M. Karamad, X. Yong, Q. Huang, D. A. Cullen, P. Zhu, C. Xia, Q. Xiao, M. Shakouri, F.-Y. Chen, J. Y. Kim, Y. Xia, K. Heck, Y. Hu, M. S. Wong, Q. Li, I. Gates, S. Siahrostami and H. Wang, *Nat. Commun.*, 2021, **12**, 2870.
20 A. Kapoor and T. Viraraghavan, *J. Environ. Eng.*, 1997, **123**, 371–380.
21 Anne Schechinger; Craig Cox. America's Nitrate Habit Is Costly and Dangerous. Environmental Working Group. October 2, 2018.
22 J. Clayworth, *Des Moines' $50M Water Nitrate Fix-It Plan*, Axios Media Inc., 2023.
23 N. Hoang Truong, J.-S. Kim, J. Lim and H. Shin, *Chem. Eng. J.*, 2024, **495**, 153108.
24 X. Lu, H. Song, J. Cai and S. Lu, *Electrochem. Commun.*, 2021, **129**, 107094.
25 Z.-Y. Wu, M. Karamad, X. Yong, Q. Huang, D. A. Cullen, P. Zhu, C. Xia, Q. Xiao, M. Shakouri, F.-Y. Chen, J. Y. Kim, Y. Xia, K. Heck, Y. Hu, M. S. Wong, Q. Li, I. Gates, S. Siahrostami and H. Wang, *Nat. Commun.*, 2021, **12**, 2870.
26 M. Zhang, Z. Zhang, S. Zhang, Z. Zhuang, K. Song, K. Paramaiah, M. Yi, H. Huang and D. Wang, *ACS Catal.*, 2024, **14**, 10437–10446.
27 Y. Fu, S. Wang, Y. Wang, P. Wei, J. Shao, T. Liu, G. Wang and X. Bao, *Angew. Chem., Int. Ed.*, 2023, **62**, e202303327.
28 G. A. Cerrón-Calle, A. S. Fajardo, C. M. Sánchez-Sánchez and S. Garcia-Segura, *Appl. Catal., B*, 2022, **302**, 120844.
29 J. Xu, S. Zhang, H. Liu, S. Liu, Y. Yuan, Y. Meng, M. Wang, C. Shen, Q. Peng, J. Chen, X. Wang, L. Song, K. Li and W. Chen, *Angew. Chem., Int. Ed.*, 2023, **135**, e202308044.
30 J. Ni, J. Yan, F. Li, H. Qi, Q. Xu, C. Su, L. Sun, H. Sun, J. Ding and B. Liu, *Adv. Energy Mater.*, 2024, **14**, 2400065.
31 W. Huang, W. Luo, J. Liu, B.-E. Jia, C. Lee, J. Dong, L. Yang, B. Liu and Q. Yan, *ACS Nano*, 2024, **18**, 20258–20267.
32 J. Sun, Y. Zhou, S. Loyaux-Lawniczak, G. Kéranguéven, C. Boudon, A. Bonnefont, L. Ruhlmann and V. Badets, *ChemCatChem*, 2024, **16**, e202400220.
33 H. Liu, J. Park, Y. Chen, Y. Qiu, Y. Cheng, K. Srivastava, S. Gu, B. H. Shanks, L. T. Roling and W. Li, *ACS Catal.*, 2021, **11**, 8431–8442.
34 A. Paliwal, C. D. Bandas, E. S. Thornburg, R. T. Haasch and A. A. Gewirth, *ACS Catal.*, 2023, **13**, 6754–6762.
35 F.-Y. Chen, Z.-Y. Wu, S. Gupta, D. J. Rivera, S. V. Lambeets, S. Pecaut, J. Y. T. Kim, P. Zhu, Y. Z. Finfrock, D. M. Meira, G. King, G. Gao, W. Xu, D. A. Cullen, H. Zhou, Y. Han, D. E. Perea, C. L. Muhich and H. Wang, *Nat. Nanotechnol.*, 2022, **17**, 759–767.
36 K. Mikami, Y. Kido, Y. Akaishi, A. Quitain and T. Kida, *Sensors*, 2019, **19**, 211.
37 J. Wei, Y. Lei, H. Jia, J. Cheng, H. Hou and Z. Zheng, *Dalton Trans.*, 2014, **43**, 11333–11338.
38 M. C. Biesinger, *Surf. Interface Anal.*, 2017, **49**, 1325–1334.
39 J. Liu, X. Sang, R. Wang, X. Li, H. Zhu, S. Du, W. You and J. Li, *J. Alloys Compd.*, 2025, **1035**, 181474.
40 I. Najdovski, P. Selvakannan and A. P. O'Mullane, *RSC Adv.*, 2014, **4**, 7207.
41 W. Go, R. A. Senthil, J. Cherusseri, A. Kumar, C. J. Moon, W. Limphirat, M. Ubaidullah and M. Y. Choi, *Adv. Funct. Mater.*, 2025, **35**, e11876.
42 W. Yuan, Y. Wu, C. Fang, X. Wang, X. Huang and C. Li, *J. Electrochem. Soc.*, 2020, **167**, 022508.
43 A. Al-Sarraj, K. M. Saoud, A. Elmel, S. Mansour and Y. Haik, *SN Appl. Sci.*, 2021, **3**, 15.
44 H. Yin, Z. Chen, S. Xiong, J. Chen, C. Wang, R. Wang, Y. Kuwahara, J. Luo, H. Yamashita, Y. Peng and J. Li, *Chem. Catal.*, 2021, **1**, 1088–1103.
45 D. Liu, L. Qiao, Y. Chen, P. Zhou, J. Feng, C. C. Leong, K. W. Ng, S. Peng, S. Wang, W. F. Ip and H. Pan, *Appl. Catal., B*, 2023, **324**, 122293.
46 Z. Song, Y. Liu, Y. Zhong, Q. Guo, J. Zeng and Z. Geng, *Adv. Mater.*, 2022, **34**, 2204306.
47 Q. Hu, K. Yang, O. Peng, M. Li, L. Ma, S. Huang, Y. Du, Z.-X. Xu, Q. Wang, Z. Chen, M. Yang and K. P. Loh, *J. Am. Chem. Soc.*, 2024, **146**, 668–676.
48 X. Zhu, H. Huang, H. Zhang, Y. Zhang, P. Shi, K. Qu, S.-B. Cheng, A.-L. Wang and Q. Lu, *ACS Appl. Mater. Interfaces*, 2022, **14**, 32176–32182.
49 H. Xu, J. Chen, Z. Zhang, C. Hung, J. Yang and W. Li, *Adv. Mater.*, 2023, **35**, 2207522.
50 Z. Fang, Z. Jin, S. Tang, P. Li, P. Wu and G. Yu, *ACS Nano*, 2022, **16**, 1072–1081.
51 Q. Hu, O. Peng, J. Liu, D. Chen and K. P. Loh, *ACS Energy Lett.*, 2024, **9**, 2303–2309.
52 M. A. Khan, I. Al-Shankiti, A. Ziani and H. Idriss, *Sustainable Energy Fuels*, 2021, **5**, 1085–1094.
53 M. Quentmeier, B. Schmid, H. Tempel and R.-A. Eichel, *ACS Sustainable Chem. Eng.*, 2024, **12**, 3876–3885.
54 B. Izelaar, M. Ramdin, A. Vlierboom, M. Pérez-Fortes, D. van der Slikke, A. Sajeev Kumar, W. de Jong, F. M. Mulder and R. Kortlever, *Energy Environ. Sci.*, 2024, **17**, 7983–7998.
55 L. Collado, A. H. Pizarro, M. Barawi, M. García-Tecedor, M. Liras and V. A. de la Peña O'Shea, *Chem. Soc. Rev.*, 2024, **53**, 11334–11389.
56 W. Gao, Y. Du, X. Liu, L. Zhang and D. Li, *Fuel Cells*, 2024, **24**, DOI: 10.1002/fuce.202400129.
57 B. M. Maxwell, R. D. Christianson, R. Arch, S. Johnson, R. Book and L. E. Christianson, *J. Environ. Manage.*, 2024, **352**, 120054.
58 X. Huang, S. Guida, B. Jefferson and A. Soares, *npj Clean Water*, 2020, **3**, 7.
59 D. Li, C. Fu, C. Wang and Q. Song, *Environ. Sci.*, 2023, **9**, 211–220.